# APPLICATION OF OPTICAL FLOW ALGORITHMS TO LASER SPECKLE IMAGING

AmirHessam Aminfar, Department of Mechanical Engineering, University of California Riverside, Riverside, CA, 92521
Nami Davoodzadeh, Department of Mechanical Engineering, University of California Riverside, Riverside, CA, 92521,
Guillermo Aguilar, Department of Mechanical Engineering, University of California Riverside, Riverside, CA 92521,
Marko Princevac, Department of Mechanical Engineering, University of California Riverside, Riverside, CA 92521,

## ABSTRACT

Since of its introduction in 1980s, laser speckle imaging has become a powerful tool in flow imaging. Its high performance and low cost made it one of the preferable imaging methods. Initially, speckle contrast measurements were the main algorithm for analyzing laser speckle images in biological flows. Speckle contrast measurements, also referred as Laser Speckle Contrast Imaging (LSCI), uses statistical properties of speckle patterns to create mapped image of the blood vessels. In this communication, a new method named Laser Speckle Optical Flow Imaging (LSOFI) is introduced. This method uses the optical flow algorithms to calculate the apparent motion of laser speckle patterns. The differences in the apparent motion of speckle patterns are used to identify the blood vessels from surrounding tissue. LSOFI has better spatial and temporal resolution compared to LSCI. This higher spatial resolution enables LSOFI to be used for autonomous blood vessels detection. Furthermore, Graphics Processing Unit (GPU) based LSOFI can be used for quasi real time imaging.

KEYWORDS : optical imaging; speckle; biomedical image processing; blood vessels

## 1. INTRODUCTION

Because of the importance of accurate blood flow visualization, various techniques for flow imaging have been proposed in medical fields such as ophthalmology, dermatology, endoscopy, and internal medicine (Stern et al., 1979). Some of these techniques are non -invasive and include methods such as Orthogonal Polarization Spectral (OPS) imaging (Groner et al., 1999), side Stream Dark Field (SDF) imaging (Goedhart et al., 2007), Laser Doppler Perfusion Imaging (LDPI) (Wardell et al., 1993)and laser speckle methods(Basak et al., 2016), such as Laser Speckle Contrast Imaging (LSCI). Among all these methods, LSCI is gaining interest because of its simplicity and ease of use.

Laser speckle effect occurs when a coherent light, such as a laser beam, illuminates a rough diffuse surface, thereby producing random interference effects. This effect is visualized by a granular pattern consisting of dark and bright spots (Rigden and Gordon, 1962). When the speckle pattern is generated on a moving object such as blood vessels, the blood flow causes fluctuations in the speckle pattern on the detector. In fluid mechanics, the phenomenon where an optical wave propagating through a medium experience irradiance (intensity) fluctuations, is referred to as optical turbulence. In LSCI, blood flow causes blurriness of image pixels, which

leads to scintillation of the intensity. Here we define *scintillation index* as:

$$S = \frac{< I^2 > - < I >^2}{< I >^2} \tag{1}$$

where $I$ denotes intensity of the optical wave, and $< >$ denotes ensembled average or a long time average. Over the years various algorithms and methods have been developed to calculate both temporal and spatial fluctuations of speckle patterns (Draijer et al., 2009; Vaz et al., 2016). These methods measure the blurriness of image pixels, which is generally centered around speckle contrast defined as:

$$\kappa = \frac{\sigma}{< I >} = \frac{\sqrt{< I^2 > - < I >^2}}{< I >} \tag{2}$$

Obviously, the speckle contrast, $\kappa$, is the same as the square root of the scintillation index defined in equation 1. When there is little or no movement in the speckle patterns, "fully developed" patterns will cause the speckle contrast (equation 2) to be equal to unity (Goodman, 1975). When there is movement in the object, the speckle pattern blurs, and the standard deviation of the intensity will be smaller than the mean intensity, thereby reducing speckle contrast. Assuming that the motion of the scattering areas of the flow is random and these random motions will decorrelate in time, the speckle contrast could be correlated to blood flow velocity. The speckle contrast is furthermore related to normalized electric field autocorrelation function $g_1(r, \tau)$ (Bandyopadhyay et al., 2005) as

$$\kappa = \frac{2\beta}{\mathrm{T}} \int_0^T |g_1|^2 \left(1 - \frac{\tau}{T}\right) d\tau \tag{3}$$

where $\beta$ is a constant which account for different optical modes in measurement. Here $\tau$ is time and $T$ is the averaging period. Typically, $g_1$ is hard to measure and therefore the intensity correlation function $g_2(\tau)$ is measured instead. Functions $g_2(\tau)$ and $g_1(\tau)$ are correlated through Siegert relation (Bandyopadhyay et al., 2005) as $g_2(\tau) = 1 + \beta|g_1|^2$. Fercher and Briers (1981) assumed that $\beta = 1$ and the measured intensity of speckles is integrated over time. Doing so, they came up with the first speckle model described as

$$\kappa = \sqrt{\frac{\tau_c}{2T}\left(1 - \exp\left(-\frac{2T}{\tau_c}\right)\right)} \tag{4}$$

where $\tau_c$ is the decorrelation time and is linked to decorrelation velocity $v_c$ defined as

$$v_c = \frac{\lambda}{2\pi\tau_c} \tag{5}$$

where $\lambda$ is the laser wavelength. Equation 4 is one of the early attempts to correlate the speckle decorrelation time to speckle contrast $\kappa$. The speckle contrast, $\kappa$, can be used to create a mapped image. In this image values of speckle contrast, $\kappa$, are different for the blood flow and surrounding tissue. This difference enables identifying the blood vessels in the image. Equation 4 has been evolving over the years. The developments have been in various methods for measurement of $\kappa$ and decorrelation time $\tau_c$ (Basak et al., 2012; Draijer et al., 2009). The newer

methodologies take into account various aspects of laser speckle patterns such as the presence of static layer on top of the blood vessels (Parthasarathy et al., 2008). Theoretical efforts were established to quantify the impact of speckle size and sampling windows on the statistics of laser speckle (Duncan et al., 2008b; Kirkpatrick et al., 2008). Moreover, studies have been done to improve laser speckle imaging algorithms. These improvements enable real-time blood flow visualization (Ansari et al., 2017, 2016a, 2016b; Humeau-Heurtier et al., 2015; Liu et al., 2008; Tom et al., 2008).

Since the normalized electric field autocorrelation function $g_1(\tau)$ is related to the mean square displacement $< |\Delta r^2| >$ of the speckle patterns (Parthasarathy et al., 2008); it can be assumed that in the blood vessels, $< |\Delta r^2| >$ is caused by the flow. Therefore, instead of using statistical behavior of laser speckle patterns, a physics based model of the blood flow can be deployed for flow visualization. In the most general form, Cauchy momentum equation can be used to describe the blood flow. However, since in many physiological conditions blood is assumed to be a Newtonian fluid (Zamir, 2016a), The Navier-Stokes equation can be used to describe the motion of the flow. The blood flow is considered pulsatile viscous flow. Assuming vessels as rigid tubes, simplified Navier-Stokes can be solved in different forms (Womersley, 1955; Zamir, 2016b) including:

$$u(r,t) = Real\left\{\sum_{n=0}^{N} \frac{i \cdot P_s}{\rho \cdot \omega}\left(1 - \frac{J_0\left(n^{\frac{1}{2}} W \cdot i^{\frac{3}{2}} \cdot \frac{r}{R}\right)}{J_0\left(n^{\frac{1}{2}} \cdot W \cdot i^{\frac{3}{2}}\right)}\right) \cdot e^{inwt}\right\} \tag{6}$$

where $u(r,t)$is the radial component of the flow, $W = R \cdot \sqrt{\rho\omega/\mu}$ is non-dimensional frequency parameter also known as the Womersley number. The angular frequency is represented by $\omega$. Viscosity and density of the fluid is represented by $\mu$ and $\rho$. The radius of the vessel is $R$, the pressure gradient magnitude is $P_s$. Bessel function of first kind and order zero is shown as $J_0$, and $i$ represents the imaginary unit.

However, the blood vessels are not rigid and the Navier-Stokes equation can be solved for pulsatile flow in an elastic tube to give (Morgan and Kiely, 1954; Womersley, 1955; Zamir, 2016b):

$$u(x,r,t) = Real\{\frac{i \cdot P_s}{\rho \cdot \omega}\left(1 - G \cdot \frac{J_0\left(W \cdot i^{\frac{3}{2}} \cdot \frac{r}{R}\right)}{J_0\left(W \cdot i^{\frac{3}{2}}\right)}\right) \cdot e^{\frac{iw(t-x)}{c}}\} \tag{7}$$

Here *c* is the wave speed and *G* is a group parameter function of Poisson's ratio, Young's modulus, diameter of tube and wall thickness of the tube. Although in some physiological conditions the assumption of Newtonian fluid is not valid; the blood flow is still governed by the Cauchy momentum equation.

In fluid mechanics, optical methods of flow visualization such as Particle Image Velocimetry, Laser Speckle Velocimetry and Background Oriented Schlieren are used to obtain better understanding of the flow field. These methodologies are based on comparing two snapshots of the flow field in different times. For example, in laser speckle velocimetry, two snapshots of the speckle patterns are taken, rather than using a single blurred image, and the displacement vectors of the

speckle pattern between the two frames are calculated. Finding displacement vectors from a pair of images is commonly referred as optical flow estimation which could be defined as the apparent motion of 2D projection of images between time steps. Cross-correlation methods are the most common methods used in computing displacement between a pair of images. In cross-correlation the whole image is divided into small windows for analysis over which the velocity can be assumed to be constant. Cross-correlation is a conventional method that is used in various applications including particle image velocimetry and laser speckle velocimetry (Dabiri, 2006). However, cross-correlation algorithms cause the analysis of speckle patterns to become much more complicated compared to speckle contrast techniques, in which speckle contrast is measured over a single image. Moreover, cross-correlation methods reduce the spatial resolution of the image as well. Because of these disadvantages, speckle contrast imaging has been more popular. With the recent developments in the computer vision especially in fields of optical flow estimation over the past two decades, more advanced and more accurate method has been developed. Atcheson et al. (2009) compared optical flow algorithms with cross-correlation algorithm using a synthetic dataset of noise backgrounds. They found that optical flow algorithms significantly increase the resolution of displacement calculations.

In this communication, a fluid mechanic approach is taken to visualize blood flow. Thus, different physical behavior of the blood flow, such as the pulsatile behavior as shown in equations 6 and 7, is used to visualize the blood flow. This was achieved by calculating apparent displacement of laser speckle patterns. As discussed earlier, when calculating displacement between a pair of images, optical flow algorithms have better resolution. Hence, optical flow algorithms were deployed to calculate the apparent displacement of image pixels. The differences in optical displacement were used to map the blood vessels. This methodology, hereafter referred to as the Laser Speckle Optical Flow Imaging (LSOFI), is similar to the laser speckle velocimetry and background oriented schlieren. In the next section the optical flow algorithms are reviewed in sufficient details followed by the section on the image acquisition. Sample results are given in section 4 followed by conclusions in section 5.

## 2. OPTICAL FLOW ALGORITHMS

The early concept of optical flow algorithms arises from James J. Gibson's (1966) work on visual stimulus provided to animals. Having two images $I(x, y, t_0)$ and $I(x, y, t_1)$ optical flow is defined as the 2D vector field describing the apparent motion of each pixel. The apparent motion computation is based on the assumption of brightness conservation, which states that the pixel intensity of the same physical point is identical in both images,

$$I(x, y, t) = I(x + \delta x, y + \delta y, t + \delta t) \tag{8}$$

As previously mentioned, when the speckle pattern is generated blood vessels, the flow causes fluctuations, which cause the intensity of the corresponding pixel in the image to change. Based on the assumption of brightness conservation (equation 8), the change of such intensities in a pair of images leads to an apparent motion of pixels. Conservation of brightness principal could be restated such as if a pixel in the picture frame is selected and the pixel is followed between the pair of images, the intensity of the pixel does not change. The material derivative can be used to describe the brightness conservation, caused by the flow, as:

$$\frac{DI}{Dt} = \frac{\partial I}{\partial t} + \frac{\delta x}{\delta t}.\frac{\partial I}{\partial x} + \frac{\partial y}{\partial t}.\frac{\partial I}{\partial y} = \frac{\partial I}{\partial t} + u.\frac{\partial I}{\partial x} + v.\frac{\partial I}{\partial y} = 0 \quad (9)$$

Equation 9 states that the apparent motion of pixel is dependent on both spatial and temporal gradient of pixel intensities. For each pixel in equation 9, there are two unknowns $u$ and $v$. Therefore, solving equation 9 requires additional constraints, which are discussed next.

2.1. Horn-Schunck method

In order to solve equation 9, Horn-Schunck (1980) introduced another set of constraint known as the smoothness constraint. Based on Horn-Schunck's approach, for slow movements, the displacement is considered smooth when the square of the gradient of velocities is minimum. Their methodology is based on the idea to minimize:

$$\int_{\Omega} (\frac{DI}{Dt})^2 + \alpha\,(|\nabla\delta x|^2 + |\nabla\delta y|^2)dxdy \quad (10)$$

where $\Omega$ represent the image domain and $\alpha$ is a factor which weights in the smoothness constraint. After basic transformations, it is shown that minimization of equation (10) is equivalent to minimization of

$$\int_{\Omega} (\frac{DI}{Dt})^2 + \alpha\,((\nabla.U)^2 + |\nabla \times U|^2)dxdy \quad (11)$$

where $U = u \cdot \hat{\imath} + v \cdot \hat{\jmath}$ is the velocity vector. Minimization of divergence of velocity $(\nabla.U)$ corresponds to the fact that the flow is incompressible, and minimization of $\nabla \times U$ signifies that the vorticity, corresponding to the blood flow field between a pair of images, is minimized.

2.2. Lucas-Kanade method

Lucas-Kanade method assumes that the motion between the two frames is slow and the displacement is constant in each small blocks of the image. Therefore, equation 9 can be assumed to hold for all pixel of a window (Lucas and Kanade, 1981). Using the weighted least– square fit and assuming a window function, $W$, to emphasize the constraint at the center of each window, the Lucas-Kanade method has the following form of solution for velocity components $u$ and $v$:

$$\begin{bmatrix} u \\ v \end{bmatrix} = \begin{bmatrix} \Sigma W^2 \left(\frac{\partial I}{\partial x}\right)^2 & \Sigma W^2 \left(\frac{\partial I}{\partial x}\right)\left(\frac{\partial I}{\partial y}\right) \\ \Sigma W^2 \left(\frac{\partial I}{\partial x}\right)\left(\frac{\partial I}{\partial y}\right) & \Sigma W^2 \left(\frac{\partial I}{\partial y}\right)^2 \end{bmatrix}^{-1} \cdot \begin{bmatrix} -\Sigma W^2 \left(\frac{\partial I}{\partial x}\right) \cdot (\frac{\partial I}{\partial t}) \\ -\Sigma W^2 \left(\frac{\partial I}{\partial y}\right) \cdot (\frac{\partial I}{\partial t}) \end{bmatrix} \quad (12)$$

2.3. Farneback method

The Gunner Farneback (2003) method does not solve equation 9. Instead it approximates a neighborhood of both frames at a time $t_1$ and $t_2$ using a polynomial function. For the case of quadratic polynomial, the intensity can be written as:

$$I_{t_1}(x) = x^T A_1 x + b_1^T x + c_1. \quad (13)$$

New signal can be constructed using a global displacement (*d*) as

$$I_{t_1}(x-d) = (x-d)^T A_1 (x-d) + b_1^T (x-d) + c_1 \\ = x^T A_1 x + (b1 - 2A_1 d)^T x + d^T A_1 d - b_1^T d + c_1 \quad (14)$$

$$I_{t_2}(x) = x^T A_2 x + b_2^T x + c \quad (15)$$

Since $I_{t_1}(x-d) = I_{t_2}(x)$, equating the coefficient in the quadratic polynomial yields to $b_2 = b_1 - 2A_1 d$ . From $b_2 = b_1 - 2A_1 d$ the transition value $d$ could be solved if $A_1$ is non-singular. In principle, equation 14 and 15 can be equated at every pixel and the solution may be obtained iteratively. Farneback (2003) noted that the pointwise solution is too noisy. Instead, the displacement may be assumed to be slow-varying and satisfies a neighborhood of values of $x$. The Farneback algorithm, combines the polynomial approximation with multi scale resolution to produce optical flow results for each pixel of the image

## 3. IMAGE ACQUISITION

In order to produce dataset for analysis of LSOFI, Laser speckle patterns were applied to the cranial bone of the mouse. The animal preparation and experimental setup have been explained in detail by Davoodzadeh et al. (2018). The images were obtained by a 12-bit CMOS camera with a rolling shutter (Thorlabs DCC1545) The camera system was attached to a microscope with 10X magnification with focus plane of 0.3mm below the surface. Laser speckle patterns were generated using a continuous wave laser of 632.8 nm wavelength coupled with beam expanders and diffusers. The resulting image had $1024 \text{ x } 1280$ pixel resolution acquired with a frame rate of 14.5 Hz. For the purpose of this study, images with the exposure time of $12.5\ ms$ were used. The result of applying LSOFI to the sample dataset are presented next.

## 4. RESULTS AND DISCUSSIONS

First, the spatial resolution of LSOFI was compared to LSCI methods. This section is followed by evaluating effect of sampling time and temporal resolution on LSOFI and LSCI. Thereafter, various filters were applied to the resulting dataset to increase the temporal and spatial resolution and help to identify the blood flow. At last, quantitative values calculated for LSOFI are presented.

### 4.1. Qualitative visualization of blood flow using optical flow algorithms

To present the visualization results, a new variable $M$ is introduced as :

$$M = \frac{1}{T}\int_0^T \sqrt{u(t)^2 + v(t)^2}\,dt \quad (16)$$

where $u(t) \text{ and } v(t)$ are horizontal and vertical motions calculated for each pixel in pair of frames and $T$ is averaging time over series of image frames. The frames are averaged primarily to increase the signal to noise ratio.

Figure 1 is visualization of $M$ when calculated using Horn-Schunck, Lucas-Kanade and Farneback optical flow algorithms. Figure 1 also shows the results of applying LSCI to the image datasets. Laser Speckle Imaging method (LSI) (Cheng et al., 2003) and Spatially Derived Contrast Using Temporal Frame Averaging (sLASCA) (Le et al., 2007) were deployed to the dataset to calculate the Laser speckle contrast $\kappa$. LSI method determines $\kappa$ over $T$ number of frames (LSI image in

Figure 1 uses T=190 frames). sLASCA method determines $\kappa$ by averaging $T$ number of Laser Speckle Contrast Analysis (LASCA) images (David Briers and Webster, 1996). In LASCA, $\kappa$ is measured in 1 image over a pixel window (sLASCA image in Figure 1 uses T=190 frames and window size of 5x5).

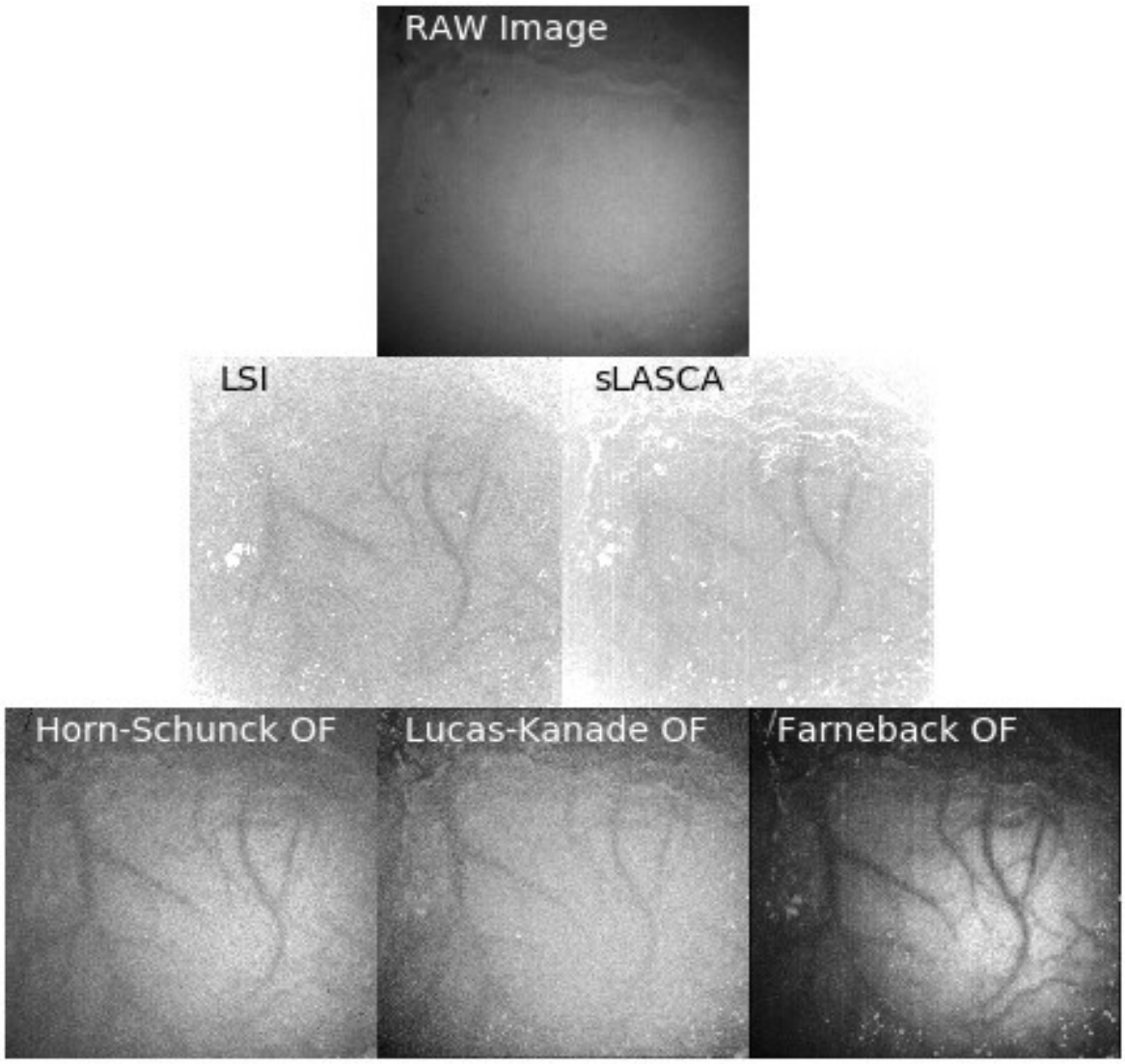


Figure 1 First row is a snapshot of the raw image obtained. The second row is the result of mapping $\kappa$ using LSI and sLASCA algorithms. The third row demonstrates the mapped value of "$M$" using Horn-Schunck, Lucas Kanade and Farneback optical flow algorithms. It can be seen that sLASCA has very low spatial resolution compared to LSI method. This could be the artifacts of using a rolling shutter camera. The LSOFI algorithms produce higher resolution images compared to LSCI imaging methods

Figure 1, clearly demonstrates that at the same temporal resolution, Horn-Schunck, Lucas-Kanade, and Farneback optical flow algorithms have higher resolution than LSCI methods. Thus, optical flow algorithms make it easier to identify and visualize the blood vessels. In the LSCI methods, sLASCA has very low spatial resolution compared to the LSI method. Therefore LSI method is compared to optical flow algorithm for this work. Among the optical flow algorithms, Horn-Schunck is more sensitive to smaller displacements. This results in more noise as compared to the Farneback algorithm, which is sensitive to all scales of motion.

As shown in equation 16, to increase the signal to noise ratio of the resulting images, $T$ number of frames were selected and averaged. When using LSI imaging method, $T$ is the number of frames used for calculation of $\kappa$. When using sLASCA, $T$ is the number of frames used for averaging the results.

To investigate the effect of averaging over the dataset, the number of frames were reduced to 20 images which corresponds to 1.37 seconds. Because of higher spatial resolution, Farneback's algorithm was chosen as the representative of the optical flow algorithms, and LSI method was chosen to represent LSCI methods. The results of applying Farneback algorithm and LSI algorithm over 20 raw images are shown in figure 2.

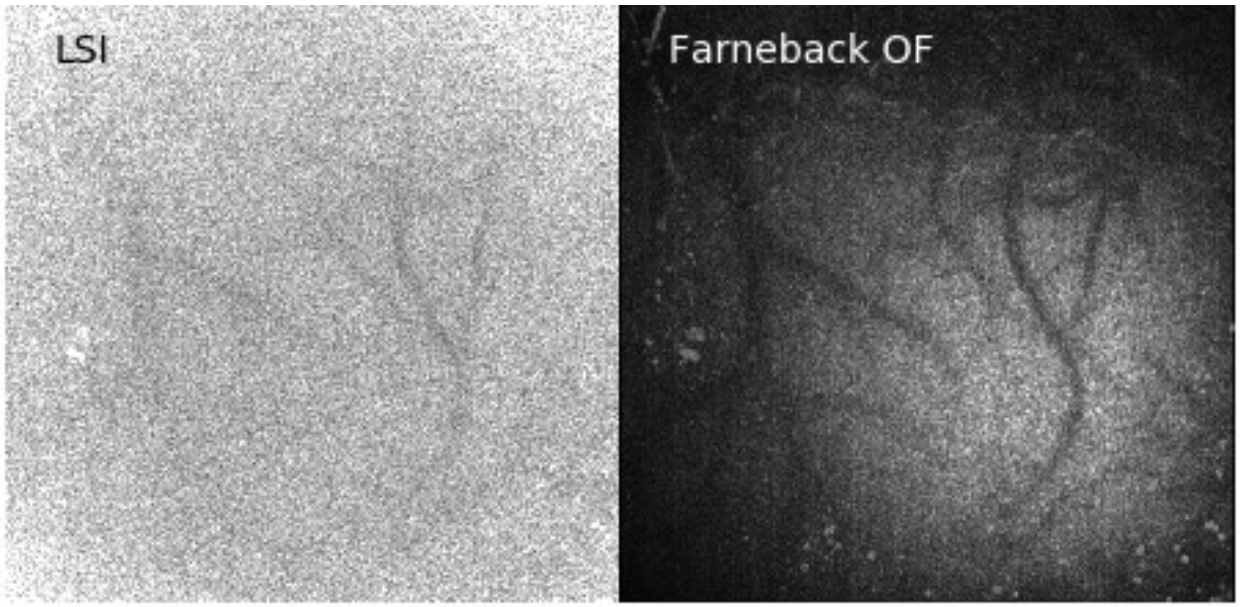


Figure 2. Image processing results of applying LSI and Farneback optical flow algorithm over 20 frames of raw-images. It can be seen that Farneback optical flow algorithm requires less images to produce a meaningful result.

Figure 2 shows that for smaller averaging, Farneback optical flow algorithm has higher resolution compared to LSI. In other words, Farneback optical flow algorithm requires a smaller number of images to produce a reasonable flow visualization as compared to the LSI method. This specification is very helpful towards quasi-real time visualization of blood vessels. Comparing Farneback's results from figures 1 and 2, that the results show that as the averaging time increases, the amount of noise in the image decreases; which leads to clearer blood vessel visualization. Figure 3 demonstrates the effect of averaging time on the output of the Farneback's optical flow algorithm.

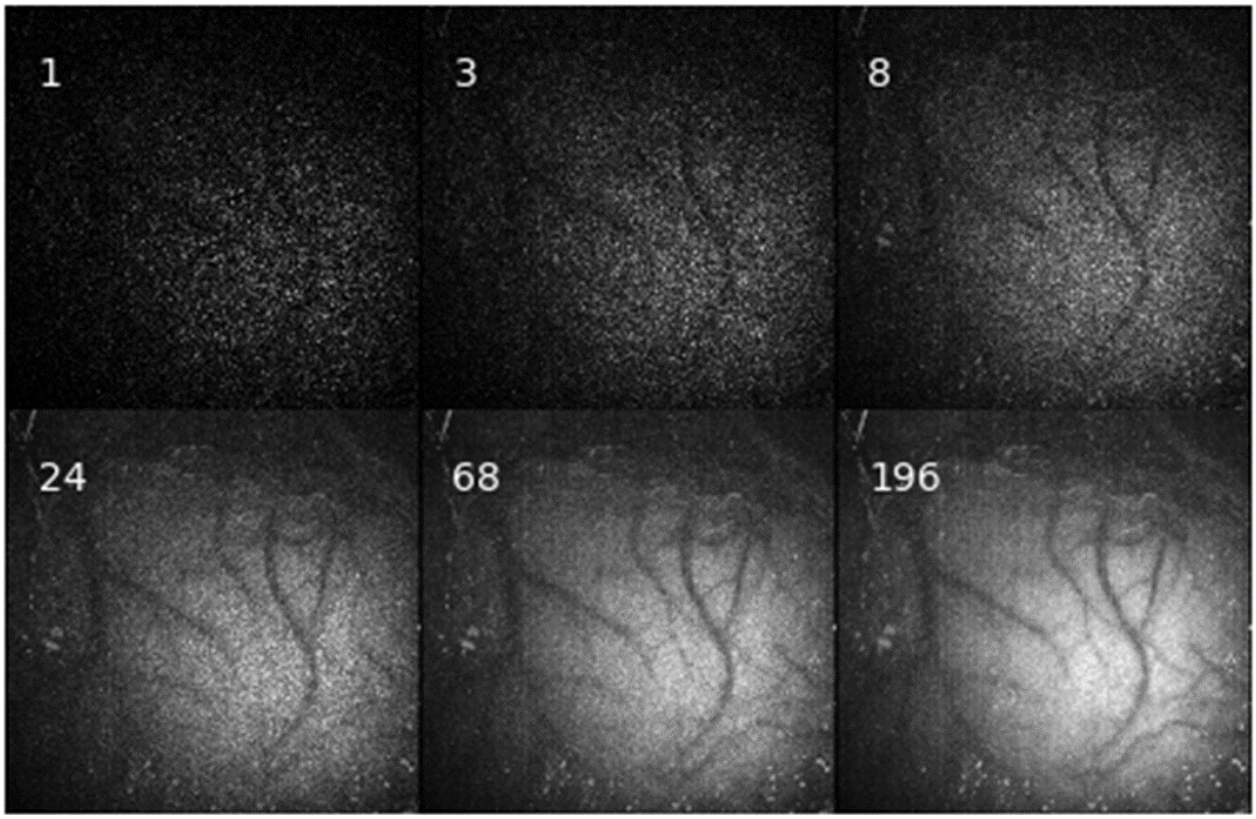


Figure 3. Image processing results using Farneback's optical flow algorithm with different averaging times. The number on the top left corner represents the number of pair of images used to process the image. As the number of data frames increases, the resolution of resulting image increases as well. It can be seen that for higher spatial resolution image, more images are required.

It can be seen from figure 3 that when the number of image pairs used for temporal averaging increases, the resolution of the output image increases. One of the optical flow algorithms advantages over LSI is that the optical flow analysis will output resulting image gradually as images are captured. LSI, which use the temporal properties of speckle patterns, require all the inputs at once to produce the resulting image.

### 4.2. . Post data processing

#### 4.2.1. Noise reduction of the images.

As shown in the previous section, optical flow algorithms, have higher resolution compared to Laser Speckle Contrast Imaging algorithms (LSCI). Moreover, it has been shown that as the number of data samples increases, the resulting image will have less noise and therefore higher resolution. However, it is not always practical to increase the number of data points to reduce the image noise. Hence noise reduction algorithms and filters could be applied to enhance the resolution. Figure 4 demonstrates the effects of the Gaussian filter and median filter to the outcomes of the optical flow algorithms. Figure 4 illustrates the result of applying filters and image noise reduction algorithms. For each of the optical flow algorithms, 10 images were used. Applying filters reduces the need for longer averaging time. It can be seen that when applying a filter, Horn-Schunck algorithm produces a higher spatial resolution image. Even though the Farneback's algorithm produces higher spatial resolution image without a filter.

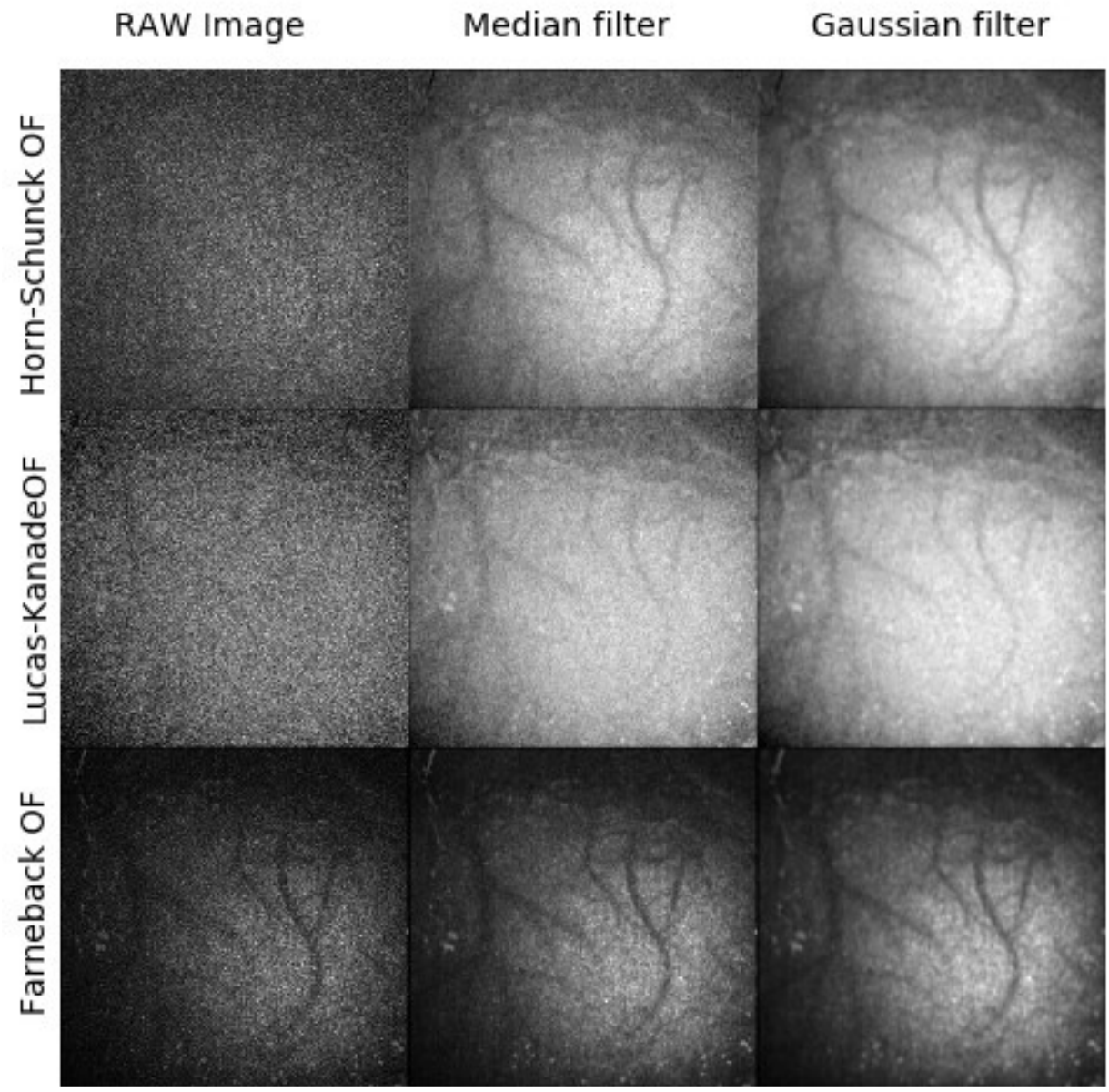


Figure 4. Result of applying a Gaussian and median filter on the optical flow result of 10 pair of images. The row indicates the optical flow algorithm used, and the columns indicate the filter applied. It can be seen that applying Gaussian and median filters to the raw results of Horn-Schunck and Lucas-Kanade optical flow algorithms lead to images with higher resolution.

#### 4.2.2. Image segmentation and identification of blood vessels

Optical flow's high spatial resolution results make it possible to identify and segment the blood vessels in the image. via image segmentation algorithms. In computer vision, Image segmentation is used to partition a digital image into different regions. By partitioning digital images into different regions, the overall analysis becomes less computationally expensive. Frangi et al.'s (1998) *"multiscale vessel enhancement filter,"* is one of the standard image segmentation algorithms, used to identify the blood vessels in a digital image. To identify the blood vessels, Frangi's filter was applied to the results of the optical flow algorithms. The results

are shown in figure 5.

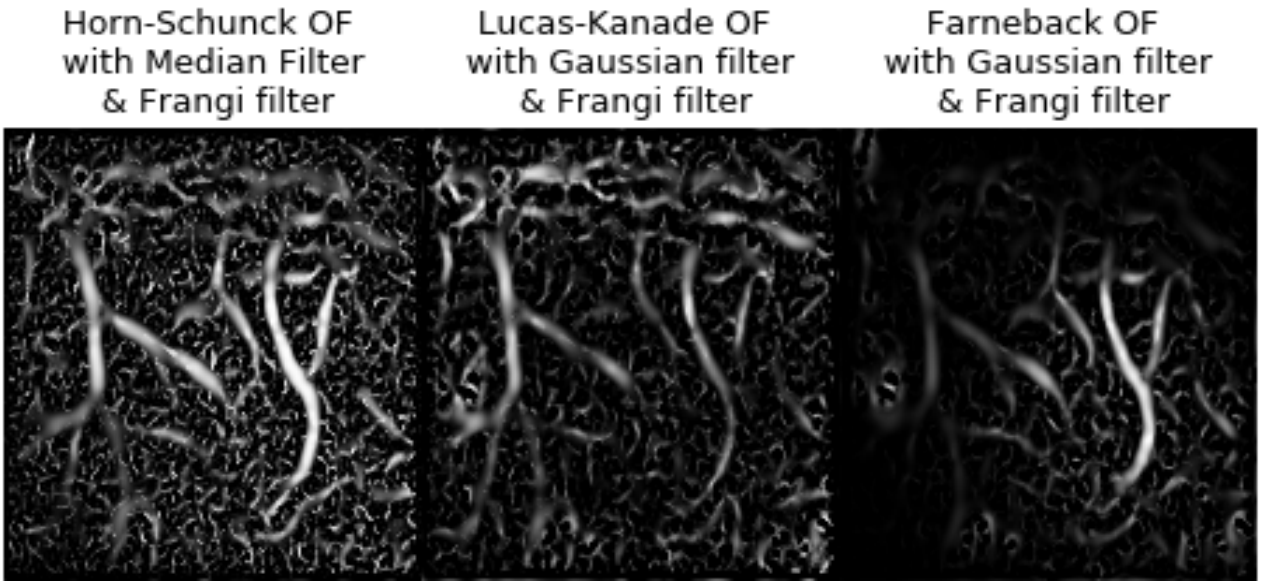


Figure 5. Results of applying a Frangi filter to the output of optical flow algorithms. The intensity of each pixel shows the vesselness calculated by Frangi filter. It can be seen for a small number of frames; the Horn-Schunck algorithm visualizes the blood vein better than other optical flow algorithms. However, the results of Farneback optical flow has less noise.

Figure 5 demonstrates that the combination of Frangi and Gaussian filtering lead to better identification of blood vessels. The intensity of the image correlates to the amount of vesselness calculated using the Frangi filter. This can later be implemented for automatic blood vessel detection using LSOFI.

### 4.3. Quantitative analysis of Laser Speckle Optical Flow Imaging

The previous sections demonstrated Laser Speckle Optical Flow imaging advantages over LSCI methods qualitatively. It also has been shown that the better resolution of LSOFI can help in developing an autonomous blood vessel detection system. However, like many LSCI methods, the correlation of quantitative value of each representing pixel with the blood velocity profile is uncertain. The quantitative unitless value of $\kappa$ is often assumed to have a correlation with the decorrelation time as explained in equations 2-5. However, this assumption has numerous issues that prevents LSCI method for becoming a quantitative measurement methodology (Duncan et al., 2008a).

In contrast to the LSCI methods, the hypothesis of the LSOFI, introduced in this paper, is physically based on the Cauchy momentum equation. Figure 6 presents the apparent displacement,$M$, for different calculation methods. The first column shows the 2D mapped displacement of the apparent motion. The second column represents the apparent motion calculated at the solid line shown in the first column. The third column represents the apparent motion calculated at the dashed line shown in the first column. The vertical dotted line in the second and third column show the approximate boundary of the vessel at the location of calculation. For the second and third column, the values of averaged displacement over 190 frames were calculated along with averaged displacement over 10 frames filtered using Gaussian and median filters. Each row

represents the optical flow algorithm used for calculation. It can be interpreted from figure 6 that when Gaussian and median filters are applied to the LSOFI results of 10 frames of images ($T$=10 in equation 16) have the same spatial resolution as when 190 frames of LSOFI results are averaged ($T$=190 in equation 16) with no filters. In simpler words, Gaussian and median filter reduce the need for additional frames. Figure 6 shows that although the magnitudes calculated by the optical flow algorithms differ, the different LSOFI algorithm produce almost the same profiles.

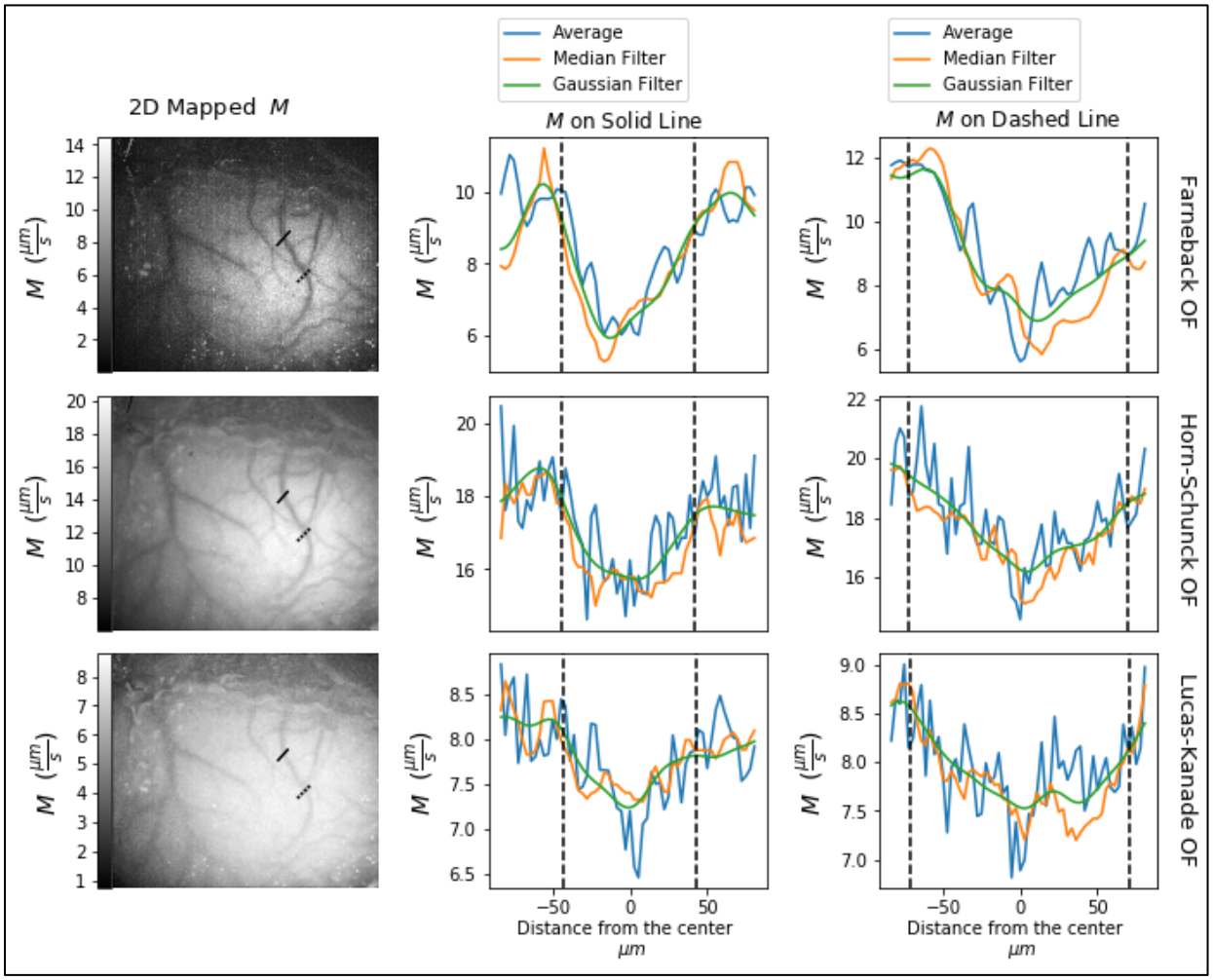


Figure 6. Quantitative analysis of displacement values. The first column presents 2D mapped values of $M$. Second and third column represent the calculated apparent motion,$M$ , at the solid and dashed lines marked in the first column, respectively. The vertical dotted line in the second and third column show the approximate boundary of the vessel at the location of the solid and dashed lines. For the second and third column, the value of averaged displacement is calculated over 190 frames ($T$=190 in equation 16) along with averaged displacement calculated over 10 frames ($T$=10 in equation 16) using Gaussian and median filters. Each row represents the optical flow algorithm used for calculating speckle displacement.

## 5. Conclusions

Laser speckle contrast imaging is known as a convenient method for visualizing flow in vessels. Common LSCI methods mapped the values of speckle contrast "$\kappa$" to produce a resulting image. In this work, a new approach of laser speckle imaging, dubbed Laser Speckle Optical Flow Imaging

(LSOFI) was introduced. In contrast with LSCI methods which uses the statistical properties of speckle patterns for flow visualization, LSOFI maps the values of the apparent displacement of laser speckle patterns. Strictly speaking, the noise caused by the blood flow is governed by Cauchy momentum equation and in some cases Navier-Stokes equation. This is in contrast with the noise displacement in the surrounding tissue which has different governing equation. LSOFI captures the speckle displacement caused by different physical behavior and creates a mapped image. It has been shown that LSOFI has advantages over LSCI methods both in temporal and spatial resolution. In other words, LSOFI can be used to produce higher resolution images compared with LSCI method using less frames. Moreover, the architecture of the LSOFI is optimal for Graphics Processing Unit (GPU) computing platforms such as Nvidia's CUDA platform(Marzat et al., 2009). Since the GPU computation increases the speed of LSOFI, the GPU enabled LSOFI could be deployed to the embedded systems such as Nvidia's JETSON to create a fast and fully functional quasi-real time blood flow imaging system.

Like LSCI methods, the substantial challenge remains if LSOFI could be used as a quantitative tool for assessing blood flow in vessels. Although the LSOFI results have the same order of magnitude as some reported values for blood flow in mouse's brain vessels, further experiments using precise velocity measurements like LDF is required to validate LSOFI as a quantitative tool for flowmetry. Nonetheless, LSOFI could be used as a valid qualitative tool for blood flow visualization

## 6. Acknowledgment

The authors would like to thank University of California at Riverside (UCR) Graduate Division for supporting the first author through the Dean's Distinguished Fellowship. This material is based on the work supported by the National Science Foundation (NSF) CBET Engineering of Biomedical Systems program under grants no. 1707190 (co-PI Princevac), NSF EAGER 1547014 and NSF PIRE 1545852 (PI Aguilar).

## 7. References

Ansari, M.Z., Cabrera, H., Ramírez-Miquet, E.E., 2016a. Imaging functional blood vessels by the laser speckle imaging (LSI) technique using Q-statistics of the generalized differences algorithm. Microvasc. Res. 107, 46–50. https://doi.org/10.1016/J.MVR.2016.04.012

Ansari, M.Z., Humeau-Heurtier, A., Offenhauser, N., Dreier, J.P., Nirala, A.K., 2016b. Visualization of perfusion changes with laser speckle contrast imaging using the method of motion history image. Microvasc. Res. 107, 106–109. https://doi.org/10.1016/J.MVR.2016.06.003

Ansari, M.Z., Kang, E.-J., Manole, M.D., Dreier, J.P., Humeau-Heurtier, A., 2017. Monitoring microvascular perfusion variations with laser speckle contrast imaging using a view-based temporal template method. Microvasc. Res. 111, 49–59. https://doi.org/10.1016/J.MVR.2016.12.004

Atcheson, B., Heidrich, W., Ihrke, I., 2009. An evaluation of optical flow algorithms for background oriented schlieren imaging. Exp. Fluids 46, 467–476. https://doi.org/10.1007/s00348-008-0572-7

Bandyopadhyay, R., Gittings, A.S., Suh, S.S., Dixon, P.K., Durian, D.J., 2005. Speckle-visibility spectroscopy: A tool to study time-varying dynamics. Rev. Sci. Instrum. 76, 93110. https://doi.org/10.1063/1.2037987

Basak, K., Dey, G., Mahadevappa, M., Mandal, M., Sheet, D., Dutta, K., 2016. Learning of speckle statistics for in vivo and noninvasive characterization of cutaneous wound regions using laser speckle contrast imaging. Microvasc. Res. 107, 6–16. https://doi.org/10.1016/j.mvr.2016.04.008

Basak, K., Manjunatha, M., Dutta, P.K., 2012. Review of laser speckle-based analysis in medical imaging. Med. Biol. Eng. Comput. 50, 547–558. https://doi.org/10.1007/s11517-012-0902-z

Cheng, H., Luo, Q., Zeng, S., Chen, S., Cen, J., Gong, H., 2003. Modified laser speckle imaging method with improved spatial resolution. J. Biomed. Opt. 8, 559. https://doi.org/10.1117/1.1578089

Dabiri, D., 2006. Cross-Correlation Digital Particle Image Velocimetry – A Review, in: A.S., Iiha A., B.B. (Ed.), Turbulência, Ed. Freire. Associação Brasileira de Engenharia e Ciências Mecânicas (ABCM).

David Briers, J., Webster, S., 1996. LASER SPECKLE CONTRAST ANALYSIS (LASCA): A NONSCANNING, FULL-FIELD TECHNIQUE FOR MONITORING CAPILLARY BLOOD FLOW.

Davoodzadeh, N., Aguilar, G., Jonak, C., Binder, D.K., Cuando, N., Aminfar, A.H., Halaney, D.L., 2018. Laser speckle imaging of brain blood flow through a transparent nanocrystalline yttria-stabilized-zirconia cranial implant, in: Tuchin, V. V., Larin, K. V., Leahy, M.J., Wang, R.K. (Eds.), Dynamics and Fluctuations in Biomedical Photonics XV. SPIE, p. 2. https://doi.org/10.1117/12.2285953

Draijer, M., Hondebrink, E., Van Leeuwen, T., Steenbergen, W., 2009. Review of laser speckle contrast techniques for visualizing tissue perfusion. Lasers Med Sci 24, 639–651. https://doi.org/10.1007/s10103-008-0626-3

Duncan, D.D., Kirkpatrick, S.J., Gladish, J.C., 2008a. What is the proper statistical model for laser speckle flowmetry?, in: Tuchin, V. V., Wang, L. V. (Eds.), . International Society for Optics and Photonics, p. 685502. https://doi.org/10.1117/12.760515

Duncan, D.D., Kirkpatrick, S.J., Wang, R.K., 2008b. Statistics of local speckle contrast. J. Opt. Soc. Am. A 25, 9. https://doi.org/10.1364/JOSAA.25.000009

Farnebäck, G., 2003. Two-Frame Motion Estimation Based on Polynomial Expansion, in: Image Analysis. pp. 363–370.

Fercher, A.F., Briers, J.D., 1981. Flow visualization by means of single-exposure speckle photography. Opt. Commun. 37, 326–330. https://doi.org/10.1016/0030-4018(81)90428-4

Frangi, A.F., Niessen, W.J., Vincken, K.L., Viergever, M.A., 1998. Multiscale vessel enhancement filtering. Int. Conf. Med. Image Comput. Comput. Interv. 130–137.

Gibson, J.J., 1966. The senses considered as perceptual systems., The senses considered as

perceptual systems. Houghton Mifflin, Oxford, England.

Goedhart, P.T., Khalilzada, M., Bezemer, R., Merza, J., Ince, C., 2007. Sidestream Dark Field (SDF) imaging: a novel stroboscopic LED ring-based imaging modality for clinical assessment of the microcirculation. Opt. Express 15, 15101. https://doi.org/10.1364/OE.15.015101

Goodman, J.W., 1975. Statistical properties of laser speckle patterns, in: Laser Speckle and Related Phenomena. Springer Berlin Heidelberg, Berlin, Heidelberg, pp. 9–75. https://doi.org/10.1007/BFb0111436

Groner, W., Winkelman, J.W., Harris, A.G., Ince, C., Bouma, G.J., Messmer, K., Nadeau, R.G., 1999. Orthogonal polarization spectral imaging: A new method for study of the microcirculation. Nat. Med. 5, 1209–1212. https://doi.org/10.1038/13529

Horn, B.K.P., Schunck, B.G., 1980. Determining Optical Flow. Artif. Intell. 17, 185–203.

Humeau-Heurtier, A., Mahé, G., Abraham, P., 2015. Microvascular blood flow monitoring with laser speckle contrast imaging using the generalized differences algorithm. Microvasc. Res. 98, 54–61. https://doi.org/10.1016/J.MVR.2014.12.003

Kirkpatrick, S.J., Duncan, D.D., Wells-Gray, E.M., 2008. Detrimental effects of speckle-pixel size matching in laser speckle contrast imaging. Opt. Lett. 33, 2886. https://doi.org/10.1364/OL.33.002886

Le, T.M., Paul, J.S., Al-Nashash, H., Tan, A., Luft, A.R., Sheu, F.S., Ong, S.H., 2007. New Insights into Image Processing of Cortical Blood Flow Monitors Using Laser Speckle Imaging. IEEE Trans. Med. Imaging 26, 833–842. https://doi.org/10.1109/TMI.2007.892643

Liu, S., Li, P., Luo, Q., 2008. Fast blood flow visualization of high-resolution laser speckle imaging data using graphics processing unit. Opt. Express 16, 14321. https://doi.org/10.1364/OE.16.014321

Lucas, B.D., Kanade, T., 1981. An Iterative Image Registration Technique with an Application to Stereo Vision 674–679.

Marzat, J., Dumortier, Y., Ducrot, A., 2009. Real-Time Dense and Accurate Parallel Optical Flow using CUDA, in: He 17th International Conference in Central Europe on Computer Graphics, Visualization and Computer Vision in Co-Operation with EUROGRAPHICS. pp. 105–112.

Morgan, G.W., Kiely, J.P., 1954. Wave Propagation in a Viscous Liquid Contained in a Flexible Tube. J. Acoust. Soc. Am. 26, 323–328. https://doi.org/10.1121/1.1907335

Parthasarathy, A.B., Tom, W.J., Gopal, A., Zhang, X., Dunn, A.K., 2008. Robust flow measurement with multi-exposure speckle imaging. Opt. Express 16, 1975. https://doi.org/10.1364/OE.16.001975

Rigden, Gordon, E., 1962. The granularity of scattered optical maser light. Proc. IRE.

Stern, M., Bowen, R., Parma, R., 1979. Laser Doppler measurements of blood flow in capillary tubes and retinal arteries. Am. J. Physiol. - Ren. Physiol. 236, F80 LP-F87.

Tom, W.J., Ponticorvo, A., Dunn, A.K., 2008. Efficient Processing of Laser Speckle Contrast Images. IEEE Trans. Med. Imaging 27, 1728–1738. https://doi.org/10.1109/TMI.2008.925081

Vaz, P.G., Humeau-Heurtier, A., Figueiras, E., Correia, C., Cardoso, J., 2016. Laser Speckle Imaging to Monitor Microvascular Blood Flow: A Review. IEEE Rev. Biomed. Eng. 9, 106–120. https://doi.org/10.1109/RBME.2016.2532598

Wardell, K., Jakobsson, A., Nilsson, G.E., 1993. Laser Doppler perfusion imaging by dynamic light scattering. IEEE Trans. Biomed. Eng. 40, 309–316. https://doi.org/10.1109/10.222322

Womersley, J.R., 1955. XXIV. Oscillatory motion of a viscous liquid in a thin-walled elastic tube—I: The linear approximation for long waves. London, Edinburgh, Dublin Philos. Mag. J. Sci. 46, 199–221. https://doi.org/10.1080/14786440208520564

Zamir, M., 2016a. Hemo-Dynamics, Biological and Medical Physics, Biomedical Engineering. Springer International Publishing, Cham. https://doi.org/10.1007/978-3-319-24103-6

Zamir, M., 2016b. Pulsatile Flow in an Elastic Tube. Springer, Cham, pp. 123–157. https://doi.org/10.1007/978-3-319-24103-6_5